Title

Estimating Nitrate Leaching to Groundwater from Orchards: Comparing Crop Nitrogen Excess, Deep Vadose Zone Data-Driven Estimates, and HYDRUS Modeling

Journal

Vadose Zone Journal, 15(11)

ISSN

1539-1663

Authors

Baram, S
Couvreur, V
Harter, T
et al.

Publication Date

2016-11-01

DOI

10.2136/vzj2016.07.0061

Peer reviewed

Published November 3, 2016

Original Research

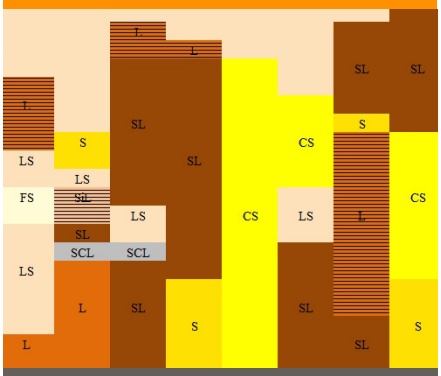

Core Ideas

- Leaching below the root zone is estimated based on eight sites of intensive vadose zone monitoring.
- Across methods N losses estimated at the annual orchard scale were in the same order of magnitude.
- Simple N mass balance provided a good proxy of the orchard scale annual N accumulation in the soil
- Under current BMP N load to groundwater is likely in the range of 60 to 100 kg N ha^{-1}.

T. Harter, J.W. Hopmans, and S. Baram, Dep. of Land, Air & Water Resources, Univ. of California Davis, One Shields Avenue, Davis, CA 95616; M. Read, D.R. Smart, Dep. of Viticulture and Enology, Univ. of California Davis, One Shields Avenue, Davis, CA 95616; P.H. Brown, and M. Kandelous Dep. of Plant Sciences, Univ. of California Davis, One Shields Avenue, Davis, CA 95616; V. Couvreur, Earth and Life Institute, Agronomy, Université Catholique de Louvain, 1348 Louvain-la-Neuve, Belgium. *Corresponding author (sbaram@ucdavis.edu),

Vadose Zone J.
doi:10.2136/vzj2016.07.0061
Received 18 July 2016.
Accepted 7 Sept. 2016.
Supplemental material

Estimating Nitrate Leaching to Groundwater from Orchards: Comparing Crop Nitrogen Excess, Deep Vadose Zone Data-Driven Estimates, and HYDRUS Modeling

S. Baram,* V. Couvreur, T. Harter, M. Read, P.H. Brown, M. Kandelous, D.R. Smart, and J.W. Hopmans

Large spatial and temporal variability in water flow and N transport dynamics poses significant challenges to accurately estimating N losses form orchards. A 2-yr study was conducted to explore nitrate (NO_3^-) leaching below the root zone of an almond [*Prunus dulcis* (Mill.) D. A. Webb] orchard. Temporal changes in water content, pore water NO_3^- concentrations and soil water potential were monitored within and below the root zone to a soil depth of 3 m at eight sites, which represented spatial variations in soil profiles within an almond orchard in California. Orchard monthly average NO_3^- concentrations below the root zone ranged from 225 to 710 mg L^{-1} with mean annual concentration of 468 and 333 mg L^{-1} for the 2014 and 2015 growing seasons, respectively. Despite the huge variability in pore water NO3− concentration between sites, the larger spatiotemporal scale N losses estimated at the annual orchard scale from surface N mass balance, vadose zone based water and N mass balance, flow calculations, and HYDRUS modeling were all on the same order of magnitude (80–240 kg N ha−1 y−1). All methods indicated that most of the N losses occur early in the growing season (February–May) when fertilizer is applied to wet soil profiles. Simple mass balance (i.e., N load applied minus N load removed) provided a good proxy of the annual N accumulation in the soil profile at the orchard scale. Reduction of N losses at the orchard scale would require alternative fertigation and irrigation practices to decrease the difference between the N load removed and the N load applied to orchards.

Abbreviations: CIMIS, California Irrigation Management Information System; NP, neutron probe; OF, objective function; SWP, stem-water potential.

Leaching of N applied to agricultural land below the effective root zone is of great concern to groundwater quality worldwide (Green et al., 2008; Hallberg, 1987; Huang et al., 2011; Viers et al., 2012). However, large spatial and temporal variability in leachable N concentrations (mainly nitrate N [NO_3^-–N]) below the effective root zone, at the scale of typical field vadose zone instrumentation, makes it difficult to accurately quantify NO_3^- losses to groundwater (Baram et al., 2016; Kurtzman et al., 2013; Onsoy et al., 2005; Turkeltaub et al., 2016). In view of emerging regulatory programs in Europe (Drevno, 2016; Tsakiris, 2015), California (Dowd et al., 2008; Harter et al., 2005), and elsewhere, there is considerable interest in the assessment and the development of methods that would enable more accurate estimates of NO_3^- losses from agricultural fields to groundwater.

Many studies have tried to quantify NO_3^- losses from agricultural land (Almasri and Kaluarachchi, 2004; Spalding and Exner, 1993). Sometimes, groundwater monitoring data are used, particularly where groundwater is shallow. Depending on the groundwater wells used, mixing and dilution processes in the aquifer may obscure or delay

the cumulative impact of NO_3^- leaching on NO_3^- level in the pumped groundwater (Green et al., 2008). To gain better understanding of agricultural land N losses to groundwater, especially in regions with thick unsaturated zones (>10 m) and potentially long travel times from low recharge rates or to get early warning monitoring systems (Fraters et al., 2016; Vrba and Adams, 2008), a need exists to monitor losses immediately below the effective root zone (usually below a depth of 1.5 m), rather than in groundwater monitoring wells.

Several studies monitored losses below the effective root zone. In some, mass balance along with in situ pore water sampling from below the effective root zone was used to evaluate NO_3^- losses under different N management practices (Li et al., 2007). In others, point measurements of changes in water content and NO_3^- concentrations across the entire vertical domain of a deep (>15 m) vadose zone were used to calibrate flow and transport models (Turkeltaub et al., 2016, 2015). However, such studies fail to address the large degree of spatial horizontal and vertical variability in NO_3^- distribution, fate, and transport below the root zone at the field or orchard scale (>0.10 km^2) (Baram et al., 2016; Botros et al., 2012; Onsoy et al., 2005).

Spatial variability in NO_3^- concentrations is driven by the inherent spatial variability of soil physical and chemical properties, by the spatiotemporal variability of water and fertilizer applications, and by the variability of nutrient uptake by individual trees (Baram et al., 2016; Giebel et al., 2006; Mohanty and Kanwar, 1994; Onsoy et al., 2005; Stenger et al., 2002). Numerous field studies have been conducted to study the spatial variability of N distribution within the root zone of agricultural fields. Typically, the observed spatial variability, along with N mass balance in the effective root zone, is used to estimate NO_3^- leaching below the root zone (e.g., Stenger et al., 2002; Ilsemann et al., 2001). Intensive core sampling along with 1-, 2-, and 3-D numerical modeling was used in few field studies of flow and transport of NO_3^- below irrigated orchards (Botros et al., 2012; Kurtzman et al., 2013; Onsoy et al., 2005; Russo et al., 2013). Results highlight the large degree of spatiotemporal variability in NO_3^- leaching below the root zone and suggest that a small fraction of the soil water (mobile water) is responsible for most of the NO_3^- transport below the effective root zone of an orchard.

Recent work by Baram et al. (2016) analyzed the spatiotemporal changes in NO_3^- concentrations in both the mobile and immobile soil phases under commercial almond orchard. Different statistical methods were applied to evaluate the effect of physical and hydrological parameters on soil NO_3^- concentrations. In addition, simple water and N mass balance was used to estimate annual N loss to groundwater at the orchard scale, a method that has high uncertainty (Healy and Scanlon, 2010). Accordingly, the objective of this work is to expand the work of Baram et al. (2016) and to compare different approaches to estimate N leaching to groundwater at the orchard scale. Specifically, we use field-scale nutrient management data and in situ vadose zone data (Baram et al., 2016) to compare field-scale annual orchard N leaching estimates obtained from water and N mass balance, the Darcy flux method, and vadose zone modeling (HYDRUS; Šimůnek et al., 1998).

Materials and Methods

Study Area

The study area is located in Madera County, CA, a few kilometers north of the San Joaquin River (36°49′15.85″ N 120°12′1.20″ W; Fig. 1) between the towns of Madera and Firebaugh. The site is located in the south–central portion of the California Central Valley, a large structural trough filled with several thousand meters of older marine and younger continental and alluvial sediments (Page, 1986). Mostly flat, with minimal topographic features, the nearly 60,000 km^2 Central Valley is home to 3.5 to 4 million ha of irrigated lands with nut, fruit, and citrus orchards being dominant among a large diversity of crops. The research sites are located on the distal alluvial fan of the San Joaquin River. The two major soil series at the sites are Danube (coarse-silty over sandy or sandy-skeletal, mesic Typic Calciaquolls) and Cajon (mixed, thermic Typic Torripsamments) sandy loams, which consist of deep, moderately to well-drained soils (6–14% clay, 67–78% sand) that formed in sandy alluvium from dominantly granitic rocks (California Soil Resource Lab, 2015). Duripans (hardpans) were formed in the region from pedogenic silica accumulation and flushing of fine soil particles (clay and silt). Weathering and pedological processes created high field-scale variability of the degree of cementation and depth to the hardpan (Kendrick and Graham, 2004; Weissmann et al., 2004). The region's elevation is 50 to 60 m asl. The climate in the region is Mediterranean with average annual high and low temperatures of 24.2 and 9.2°C, respectively, and an average annual precipitation (1928 to 2010) of 311 mm that falls predominantly during the winter season (November–March). The site is located above a phreatic aquifer, and the depth to the water table is ~30 m. The main recharge to the aquifer is the San Joaquin River, but percolation of seasonal rainwater and leaching of irrigation water from irrigated land also play a role. The region is intensively cultivated with grape (*Vitis vinifera* L.), almond, and pistachio (*Pistacia vera* L.). This area is classified by the California Department of Water Resources as a hydrogeologically vulnerable area (California Environmental Protection Agency, 2000).

A 16-yr-old, 16-ha (40 acre) commercial almond orchard was chosen to study the movement of NO_3^- below the root zone at the orchard scale. The trees are planted on trapezoidal berms (0.9 m (3 ft.) wide by 0.2 m high) at intervals of 5.5 m (18 ft.) along the berm and with 7.3 m (24 ft.) driveways between tree rows. The orchard is planted with Nonpareil and Carmel almond cultivars on alternating rows for a total of 55 rows with 73 trees per row.

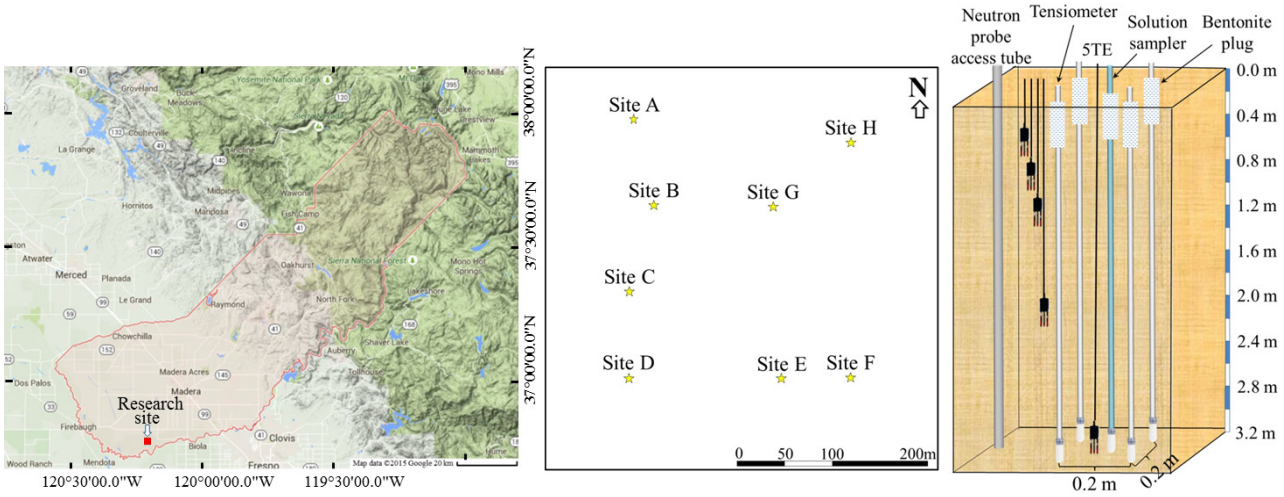

Fig. 1. The geographic location of the research site (left panel), the monitoring sites at the orchard (center panel), and the monitoring setup at each site (A–H) (right panel).

Each tree is irrigated by one 38 to 45 L h^{-1} microsprinkler (Fan-Jet, Bowsmith), with a 3-m wetting radius (total wetted area: 11 ha, 71% of the orchard).

The orchard was irrigated once a week with locally pumped groundwater. In 2014, the pumped groundwater contained NO_3^- concentration of 35 mg L^{-1}, while in 2015 the NO_3^- concentration decreased to 10 mg L^{-1} because of the addition of a new deep-pumping well. Irrigation duration ranged from 10 h early in the season (March) to 48 h later in the season (July–September). Urea–ammonium nitrate solution fertilizer (UAN, 32% N by weight) was used in all fertigations. Fertigations followed best management practices guidelines, which recommend three to four fertilizer applications with different loads following fruit development throughout a growing season (California Almond Sustainability Program, 2016). Accordingly, the orchard received 50 to 112 kg N ha^{-1} for each fertigation. Prior to bloom, compost was applied to the orchard.

Monitoring Approach and Field Instrumentation

A grid-based soil survey was used to assess the spatial variations in soil layers at the orchard. For that purpose, 16 boreholes were augered between trees to depth of 3.4 m using a soil hand auger (AMS Inc.). Over 230 borehole samples were analyzed for particle size distribution using the hydrometer method (Ashworth et al., 2001). Rooting depth was estimated from three 3-m-deep soil pits. Most of the roots (>90%) were in the upper 1 m of the profile; few roots were observed below 1 m, visible to a maximum depth of 2.0 to 2.5 m. Accordingly, hereafter we refer to the upper 1 m of the root system as the effective root zone.

Porewater samplers (solution samplers) and tensiometers were built by attaching round-bottom, tapered-neck ceramic cups (2.2 cm o.d. and 7.0-cm-long 1 bar; Soilmoisture Equipment Corp.) to 1.9-cm-i.d. (3/4 inch) to 2.9-, 3.0-, and 3.1-m-long PVC pipes and attaching a 1.27-cm-i.d. (1/2 inch), 10-cm-long transparent Plexiglas tube to the top. The Plexiglas allowed for real-time monitoring of the water level inside the tensiometers and was sealed at the top by a self-sealing rubber septum. For the tensiometers, an electronic pressure transducer (part No.26PCAFA6D, Honeywell) was connected to the top of the Plexiglas pipe. Flexible electrical "spaghetti" tubes (0.1 cm i.d.; Cope Plastics, Inc.) were guided to the bottom of each solution sampler, allowing pore water sampling using a vacuum pump.

Based on the soil survey information and the observed rooting depth, eight locations were chosen for soil layering characterization (Fig. 2). In February 2014, each of those sites was instrumented with five 5TE soil moisture sensors (0.3, 0.6, 0.9, 1.8, and 2.9 m) (Decagon Devices, Inc.), a solution sampler, and four tensiometers. All instruments were installed inside a 3.2-cm (1.25 inch)-diam. borehole, backfilled with soil slurry, and sealed with bentonite along the top 20 cm of the soil. The tensiometers were installed 20 cm apart as two couples at depths of 2.8 and 3.0 m located 0.9 and 1.1 m away from the center of the berm with the solution sampler and 5TE installed between them at depth of 2.9 m. A total of nine additional solution samplers were installed at a depth of 2.9 m (Fig. 1) in January 2015. In September 2014, a single 3-m-long (5.8 cm i.d. [2 inch]) PVC neutron probe (NP) access tube was installed at each one of the monitoring sites.

To record irrigation height and to compare irrigation uniformity along the orchard, eight flow meters (part No. 36M201T.1, Netafim-USA) were installed at the start of the irrigation line at

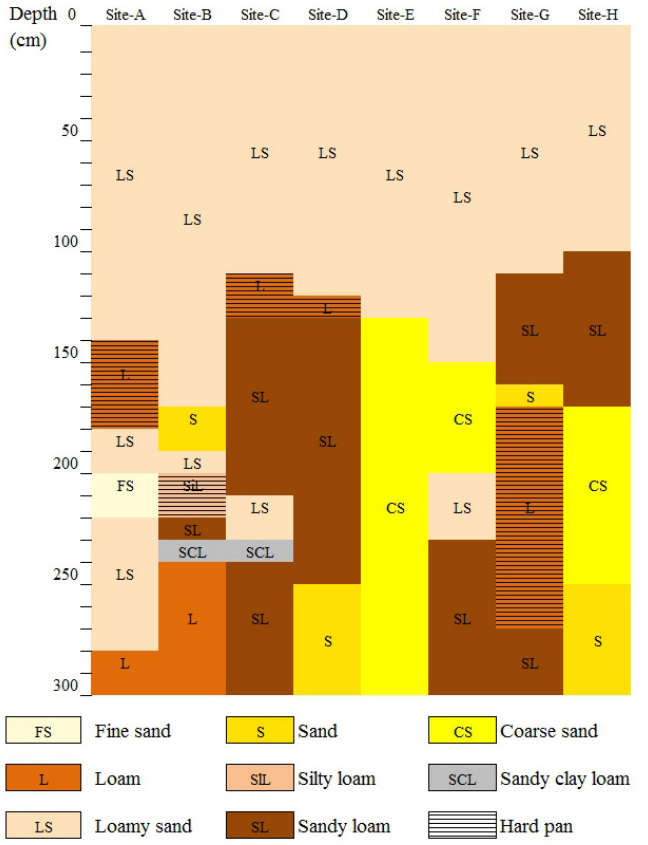

Fig. 2. Soil profiles under the monitored sites in the orchard (modified from Baram et al., 2016).

each row in which instruments were installed. Precipitation was recorded at the field every 15 min using a rain gauge (Davis 7852 Rain Collector II, Davis Instruments).

Porewater was sampled every 1 to 2 wk when wet soil conditions extended to depth of 3 m and up to 4 wk apart when the soil at depth of 3 m was dry. Following each fertigation event, pore water was sampled for three consecutive days. To minimize the effect of pore water sampling on the adjacent tensiometers readings, pore water was sampled after applying suction to the solution sampler for 3 to 12 h. Neutron probe (model 503DR, CPN, Inc.) readings were taken using 0.3-m depth intervals, every 1 to 4 wk. Count ratios between the readings in the protective shield of the NP and the readings in the soil were used to reduce the effects of temperature and drift from electronics (Yao et al., 2004). At each depth increment, four readings were taken, and the average of the four was used to determine the volumetric water content using a calibration curve that was determined from 45 undisturbed core samples (coefficient of determination $R^2 = 0.96$).

All the tensiometers and 5TE sensors were connected to CR1000 (Campbell Scientific) and NeoMote (Metronome Systems LLC) data loggers. Water content and tension readings were taken every 15 min throughout the year.

Irrigation water was collected in vials via three drippers that were inserted into the microsprinkler irrigation lines. All water samples were stored in polypropylene bottles and kept on ice until laboratory testing after passing through a 45-μm glass fiber filter. Water samples were analyzed for NO_3^- concentrations using vanadium(III) reduction (Doane and Horwáth, 2003), NH_4^+ concentrations as indophenol blue complex using salicylate (Kempers and Kok, 1989), and total N concentrations using the persulfate digestion method (APHA 4500-N C) (American Public Health Association, 1998).

Nitrogen Losses

Annual Nitrogen Accumulation in the Soil Profile

Mass balance was used to calculate the annual N load accumulated (excess-N) in the soil profile from unutilized N fertilizer. The annual excess N was calculated as the difference between N application (N mass in applied fertilizer including organic amendments and groundwater) and tree N uptake (N mass in wood, kernel, shell, and hull). Nitrogen uptake was estimated based on yield measurements in nine different rows and a 23 kg N ha^{-1} for vegetative growth (Silva et al., 2013). Nitrogen content in the kernels, shells, and hulls was analyzed through oxidation of the sample by flash combustion using TruSpec C/N Analyzer (LECO Corp.). Nitrogen from precipitation and atmospheric N losses were not accounted for. The N stock in the effective root zone, constructed manly of NO_3^-–N (accounting for the solid phase and the mobile and immobile dissolved phases), was also not accounted for in the calculations since it was very low and did not change significantly (Baram et al., 2016).

Nitrogen Leaching Below the Root Zone

The mass of N (M [M T^{-1} L^{-2}]) (as NO_3^-–N) leaching below the root zone was calculated using three methods: (i) vadose-zone-based water and N mass balance, (ii) Darcy flow calculations, and (iii) HYDRUS inverse modeling. In the first two methods, the annual NO_3^-–N mass lost through leaching is calculated by multiplying water leaching by NO_3^-–N concentration in the soil solution:

$$M = \sum_{i=1}^{n} L_i C_i \Delta t_i A \quad [1]$$

where L is the water leaching flux below 3 m soil depth (cm [week or day]$^{-1}$), C is the average NO_3^-–N concentration in the leaching water at that depth (g m^{-3}), Δt is a given time period (week or day), and A is the horizontal surface area of an hectare (10,000 m^2 ha^{-1}).

The two methods differ in the way they calculate water leaching (L): in the mass balance method, L is obtained from a field-scale water mass balance (Eq. [2]); in the Darcy flux method, locally measured hydraulic gradients and hydraulic conductivities below the root zone are used (Eq. [3]).

Water Mass Balance

The volume of water leaching below 3 m soil depth was calculated for each site using the following equation:

$$L_i = (\text{Ir} + \text{rain}) - (\text{ET}_c) - (\Delta S) \quad [2]$$

where Ir and rain are the cumulative irrigation and precipitation, respectively (cm), ET_c is the cumulative water loss through evapotranspiration (cm), ΔS is the change in soil water storage (cm). The ΔS value was calculated using two sets of instruments: the 5TE data and NP data. In the 5TE-based storage calculations, the lithological profile was accounted for. The ET_c value was estimated based on ET_0 data from California Irrigation Management Information System (CIMIS) Station No. 188 (CIMIS, 2014), which was multiplied by crop coefficients (K_c) based on the work of Goldhamer (2012). In this method, both the water flux (Eq. [2]) and N leaching below 3 m soil depth (Eq. [1]) were solved weekly (i.e., Δt = 1 wk; n = 52).

Darcy Method

In the Darcy method, the water leaching flux below a depth of 3 m was calculated daily using the empiric law of Darcy:

$$L = K\frac{\partial h}{\partial z} \quad [3]$$

where K is the hydraulic conductivity (cm d^{-1}), h is the total hydraulic head (cm), and z is the elevation above a vertical datum (cm). The hydraulic conductivity was calculated daily as a function of the matric potential [$K(\psi)$] using the van Genuchten (1980) Mualem (1976) formula:

$$K(\psi) = K_s\left(\frac{1}{\left[1+(\alpha|\psi|)^n\right]^{1-\frac{1}{n}}}\right)^{\frac{1}{2}}\left\{1-\left[1-\left(\frac{1}{\left[1+(\alpha|\psi|)^n\right]^{1-\frac{1}{n}}}\right)^{\frac{n}{n-1}}\right]^{1-\frac{1}{n}}\right\}^2 \quad [4]$$

where K_s is the hydraulic conductivity at saturation (cm d^{-1}), ψ is the matric potential (cm), and α (cm^{-1}) and n (–) are empirical parameters that are related to the inverse of the air entry pressure and the pore-size distribution, respectively. The field-gathered matric potentials at depths of 2.8 and 3.0 m data and the water content at depth of 2.9 (5TE and the NP) were used to generate eight in situ retention curves for each monitoring site. The RETC computer code (van Genuchten et al., 1991) was used to fit the α and n parameters for each curve.

The K_s values of the soils at depth of 2.8 m in each site were estimated using the permeameter method. A one-way valve (part No. H4095012V (V-S), Hudson Valve Inc.) was connected to a 3-m-long, 1.9-cm-i.d. (3/4 inch) PVC pipe placed at the bottom of a 7.62-cm (3 in) borehole and filled with water, keeping constant head at the bottom of the borehole. Once the infiltration rate did not change over several consecutive readings, K_s was calculated using the following equation (US Bureau of Reclamation–Denver, 1990):

$$K_s = \frac{Q}{2\pi h^2}\left\{\ln\left[\frac{h}{r}+\sqrt{\left(\frac{h}{r}\right)^2+1}\right]-\left[\frac{\sqrt{\left(\frac{h}{r}\right)^2+1}}{\frac{h}{r}}\right]+\frac{1}{\frac{h}{r}}\right\} \quad [5]$$

where Q is steady flow rate (mL s^{-1}), h is height of constant water head in the borehole (cm), r is borehole radius (cm), and π is 3.14. To ensure that the field-estimated K_s values were reasonable, two steps were taken: (i) the values were compared with the expected value for the specific soil type (Clapp and Hornberger, 1978) and, (ii) the values were decreased, when needed, such that calculated Darcian leaching flux in the 2 wk following flood irrigation (periods with high flux) did not exceed the applied water (irrigation plus rain) at that time frame. In the latter approach, we assumed that the matric potential readings by the tensiometers and the corresponding hydraulic gradient between them were accurate; hence, the K_s value had to be lowered to comply with mass balance conservation. Similar to the mass balance method, N leaching below the root zone was calculated daily using Eq. [1] (i.e., Δt = 1 d; n = 365).

Inverse Modeling Framework Methodology

The third estimate is based on calibrating a physically based, unsaturated flow model against field measurements. The HYDRUS 1D code (Šimůnek et al., 1998) along with MATLAB software (MathWorks, 2012) were used as an inverse modeling framework to estimate soil hydraulic properties, water leaching, and NO_3^- transport at soil depth of 3 m. Soil water flow was calculated with the Richards equation (Richards, 1931) coupled with Feddes et al. (1978) root water uptake model (using: h2 = −600 cm, h3 = −8000 cm, and ω_c = 0.3) and Vrugt et al. (2001) one-dimensional root distribution model (using: z* = −10 cm, z0 = −145 cm, and pz = 0 [linear]). Nitrate uptake followed the mass flow of water uptake, and its transport across soil layers was calculated with the convection–dispersion equation (using a diffusion coefficient of 0.18 cm^2 d^{-1} and a dispersion length of 5 cm (for more information see Gärdenäs et al., 2005).

We used the inverse modeling approach to calibrate soil hydraulic parameters using measured soil water content, soil matric potential, and their temporal changes as calibration targets. The Genetic Algorithm, FMinSearch, and FMinCon optimizers (available in MATLAB optimization toolbox) were all used to search for the soil hydraulic parameter set that best fit the field observations (for more information on the optimizers see Coleman and Li [1996]), Lagarias et al. [1998]), and Whitley [1994]). A set of parameters, θ_s, α, n, and K_s of the van Genuchten (1980) equation, was optimized for the bulk soil in the profile (high permeability) and another set of parameters, α, n, and K_s, for soil horizons such as hard pans

(lower permeability) for a total of seven parameters. The parameter θ_s scales soil water storage capacity, which was a key observation in the bulk soil but not in thinner hardpan layers, which do not store much water. Hence, we only optimized θ_s in the bulk soil to limit the complexity of the optimization problem. An initial population of 100 parameter sets (P) was randomly picked from a bounded parametric space (see Supplemental Table S1).

For each tested parameter set (P), differences between simulated and measured observations (residuals) were quantified with a second-order moment of the residuals, which gives more weight to large errors. Three steps were taken to obtain a single score of performance of the fit, the so-called objective function (OF). First, the residuals were averaged within each observation type. Uniform weights were used for matric potentials (hPa), while weights proportional to the amplitude of the observation were used for temporal changes of water content (cm cm^{-1}) of storage (i.e., integrated water content over the top 1 m in cm units), and of matric potential (hPa):

$$\mu_t = \sum_{i=1}^{N_t} |s_{t,i} - m_{t,i}| w_{t,i}$$

where μ_t is the average water status or status change for the observation type t (e.g., matric potential or matric potential change), N_t is the total number of residuals for observation type t, $s_{t,i}$ is the ith simulated observation of type t, $m_{t,i}$ is the ith measurement of type t, $w_{t,i}$ is the weight associated to the ith residual of observation type t (it equals $1/N_t$ in case of uniform weights, and

$$\frac{|s_{t,i}| + |m_{t,i}|}{\sum_{i=1}^{N_t} |s_{t,i}| + |m_{t,i}|}$$

in case of weights proportional to the amplitude of the observation). The interest of the weighting proportional to the signal fluctuation, for instance when fitting water-content change, is that large changes are attributed more weight, while small changes that could be due to scattering in measurements are of lesser importance in the OF. Also, perfectly matching a flat water-content signal does not significantly improve the OF value with this method, as we want to focus the optimization effort on the reproduction of water-content fluctuations. However, changes in both measured and simulated water contents intervene in the weights. Hence, if the measured water content does not fluctuate but the simulated water-content fluctuates a lot, the weight will be high, and the error will not be neglected.

Second, the average residuals were normalized by the corresponding average water status or average water status change (e.g., the average residual of matric potential was normalized by the average matric potential, but the average absolute residual of matric potential change was normalized by the average absolute matric potential change) to express errors with the same nondimensional units:

$$\mathrm{OF}_t = \frac{\mu_t}{\sum_{i=1}^{N_t} |m_{t,i}| w_{t,i}}$$

Third, the nondimensional errors OF_t were aggregated into a single OF value with arbitrary weights (reported in Supplemental Table S2).

$$\mathrm{OF} = \sum_{t=1}^{T} \mathrm{OF}_t W_t$$

where W_t (%) are weights attributed to each type of observation, and T is the total number of observation types. Different weights were chosen until optimal optimization was achieved at each site.

The value of the weights differed between sites and summed to 100%. After the OF value was obtained, the optimizers picked a new set of parameters P according to their respective algorithms. In the optimization process, the global optimizer was used first to search for better parameter sets, and then local optimizers were used to refine the solution locally. Both methods were used until they converged to a minimal value of the OF. In the optimization process, data of 8 to 12 mo were used for calibration out of the 24 mo of data. Daily observation times were selected at three depths for water content (30, 60, and 90 cm depth), integrated over the first meter of soil for water storage, and at two depths for soil matric potential (280 and 300 cm depth). Water content changes at intervals of 1, 2, 4, and 40 d were selected. Intervals of 1, 4, and 40 d were selected for water storage change and 5, 10, and 40 d for soil matric potential change. Selecting different time intervals allowed better constraining of the fit over both short and long time frames.

Top boundary conditions (precipitation and irrigation) were based on field measurements, while evapotranspiration was defined based on $\mathrm{ET_o}$ data from CIMIS combined with K_c parameters of Goldhamer (2012) to transition linearly from the low plateau (K_{c1}) to the high plateau (K_{c2}), yearly. The lower boundary condition was set as free drainage at 4.4 m depth in order not to directly affect the estimated leaching at 3.0 m.

The monitored matric potentials and water contents were used to generate the initial soil matric potential profile. Initial matric potentials between observation depths were linearly interpolated. In the modeling, the in situ water-content measurements were grouped by soil type (1, loamy sand; 2, loam and sandy loam; 3, coarse sand). Linear regressions between NP and 5TE measurements were characterized for each group ($R^2 > 0.75$) to adjust the calibration of 5TE sensors so that they match NP observations but maintain a high time resolution. The loamy sand of Site 5

displayed a significantly different relation and was thus recalibrated separately.

Results

Irrigation and Rain

The 2014 and 2015 growing seasons began after exceptionally dry winters (Table 1). Hence, in 2014 and 2015, prior to bloom, the orchard was flood irrigated for 24 h to refill the soil profile. During the growing season (February–October) the weekly irrigation equaled the evapotranspiration demand. An exception to that trend occurred from August through mid-September when the orchard was dried for periods of 20 to 25 d to enable harvest. In 2014, the orchard was also flood irrigated for 24 h after it was harvested (October). Total evapotranspiration in 2014 and 2015 growing seasons was nearly identical (Table 1). In 2014 and 2015, the annual sums of irrigation and precipitation in the orchard were 25.7 and 6 cm larger, respectively, than the estimated annual cumulative evapotranspiration (ET_c) during these years (Table 1), suggesting some water leaching at the orchard scale.

Nitrate Application, Uptake and Concentrations in Pore Water, Field-Scale Nitrogen Mass Balance

In both growing seasons, similar loads of N were applied to the orchards through chemical fertilizer and compost applications (240 and 45 kg N ha^{-1}, respectively). Nonetheless, the total load applied in 2014 was higher because of higher NO_3^-–N concentration in the irrigation water (Table 1).

Yield measurements indicated up to 1.4 times difference in kernel loads per row within a season. The N content in the kernels at the end of the growing seasons ranged from 3.16 to 6.6% N. Hence, N removal between trees within an orchard varied by as much as a factor of two. Nonetheless, the orchard average annual difference between N applied and N removed from the orchard (excess N) was similar for 2014 and 2015 (98 and 86 kg N ha^{-1} y^{-1}, respectively). Assuming that excess N was diluted by the excess applied water (annual cumulative sum of irrigation and rain minus annual cumulative sum of evapotranspiration [ET_c]), the effective N concentration in the soil profile across the orchard would be ~38 and ~143 mg NO_3^- L^{-1} for the 2014 and 2015 growing seasons, respectively.

Between February 2014 and February 2016, 310 pore water samples were collected from depth of 2.9 m across the monitoring sites in the orchard. Detailed description of the NO_3^- concentrations and trends can be found in Baram et al. (2016). In general, throughout the monitoring period, the NO_3^- concentrations across the orchard differed by two to three orders of magnitude (Fig. 3). The orchard mean NO_3^-–N concentration in 2014 and 2015 remained around an order of magnitude higher than the drinking water standard of 10 mg L^{-1} (109 and 75 mg NO_3^-–N L^{-1}, respectively). Postharvest and late-winter flood irrigation resulted in deep (>3 m) drainage.

Table 1. Water balance and nitrogen loads applied and harvested.

	1 Feb. 2014 through 31 Jan. 2015	1 Feb. 2015 through 31 Jan. 2016
Rain (cm)	15.6	20.4
Irrigation (cm)	120.9	100.8
Evapotranspiration (cm)	110.8	115.2
Nitrogen applied (kg N ha^{-1})†	335	296
Nitrogen harvested (kg N ha^{-1})‡	237	210

† Taking into account N in compost, chemical fertilizer, and irrigation water (groundwater).
‡ Taking into account measured kernels N content and 23 kg N ha^{-1} for vegetative growth (Silva et al., 2013).

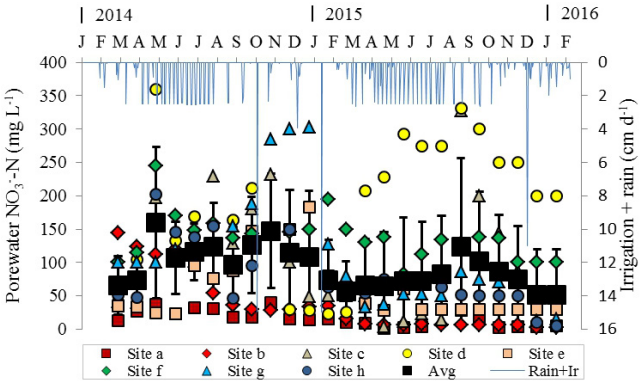

Fig. 3. Monthly average pore water NO_3^-–N concentrations at soil depth of 2.9 m in each one of the eight monitoring sites along with the orchard monthly average concentration (Avg) from 2014 through 2016. Irrigation and rain applied also presented.

Water Flux below the Root Zone

Big differences were observed between water-content measurements by the 5TE sensor and by the NP at soil depth of 2.9 m, especially under dry soil conditions. In sites with sandy loam to loamy soils, the volumetric water-content measurements by the 5TE sensors were 40 to 60% lower than the water-content measurements by the NP. In contrast, in sites with sandy soil, measurements by the 5TE sensors were 1.5 to 3.6 times higher than the water-content measurements by the NP. Despite these differences, both measurement methods indicated similar temporal changes in the volumetric water content (Table 2).

Regardless of the water-content sensor, all three methods (i.e., water mass balance, Darcy flux, and HYDRUS modeling) indicated high downward flux during the winter and early spring (December through late April), especially following flood irrigation events. Later in the season (May–October) the soil profile dried and the downward flux approached zero (less negative) and even became positive, indicating upward water flux from the moisture pool in the deeper vadose zone (Fig. 4a). In 2014, the

Table 2. Yearly average water content at depth of 2.9 m below the eight monitoring sites measured by neutron probe (NP) and 5TE sensors.

Site	Water content		Soil
	5TE	NP	
	$cm^3\ cm^{-3}$		
A	0.146	0.346	Loam
B	0.195	0.323	Loam
C	0.203	0.323	Sandy loam
D	0.108	0.030	Sand
E	0.074	0.051	Sand
F	0.125	0.314	Sandy loam
G	0.123	0.286	Sandy loam
H	0.120	0.036	Sand

calculated average cumulative flux varied greatly between the three methods (12.0–32 cm yr^{-1}), while less variability between methods was observed in 2015 (12.6–22 cm y^{-1}) (Fig. 4b).

Darcy flux calculations showed that the yearly average fluxes to below 3 m soil depth at the orchard, based on 5TE data and on NP data, were fairly similar (12.0 vs. 14.9 cm y^{-1} in 2014, respectively, and 12.6 vs. 18.7 cm yr^{-1} in 2015, respectively). Similar to the Darcy method, the yearly average fluxes calculated based on the water mass balance approach (Eq. [2]) and NP and 5TE data were comparable (18.3 vs. 15.1 cm yr^{-1}). The monthly water fluxes calculated by the calibrated HYDRUS model were in good agreement with the fluxes calculated by the other methods (Fig. 4a). Nonetheless, through most of the year, the orchard average monthly flux calculated by the HYDRUS model was slightly higher than the flux calculated by the other methods, resulting in higher cumulative flux (Fig. 4).

In both growing seasons, the spatial variation in the water flux across the orchard calculated by the Darcy and water mass balance methods remained in the same range (1–33 cm y^{-1}), while the range of fluxes calculated by the inverse modeling were smaller (22–30 cm y^{-1} in 2014, excluding Site E, and 15–36 cm y^{-1} in 2015). However, despite the similarity in flux range across methods, at an individual site, 5TE- and NP-based calculations indicated up to threefold difference in the flux values. The biggest differences were observed between the 5TE and NP-based fluxes at Site E (15–20 vs. 0.35–1.0 cm y^{-1}, respectively). Similar to the other methods, the modeling indicated exceptionally high fluxes in Site E during the 2014 and 2015 growing seasons (56 and 30 cm y^{-1}, respectively).

Nitrate Flux below the Root Zone

The orchard average NO_3^- fluxes below the effective root zone across all three calculation methods were of the same order of magnitude (80–240 kg N ha^{-1} yr^{-1}). For most sites, Darcy flux calculations with 5TE data had the lowest NO_3^- fluxes, while water-mass-balance-based calculations had the highest flux (Fig. 5).

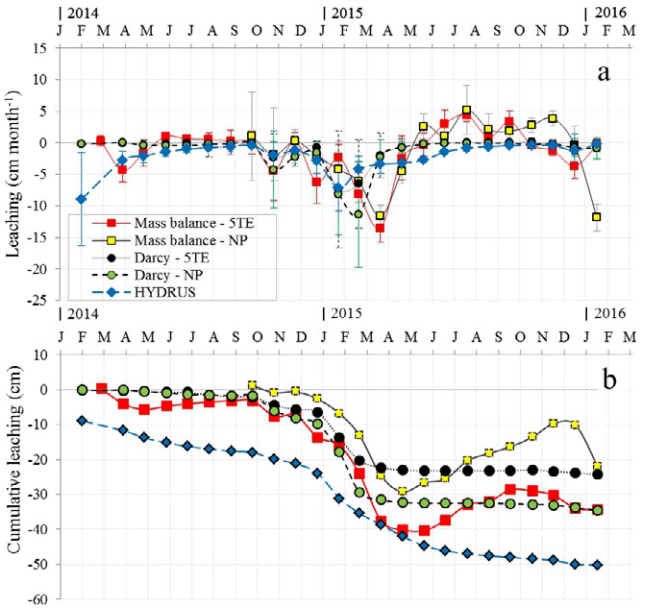

Fig. 4. (a) Average monthly leaching flux and (b) cumulative flux at soil depth of 3 m calculated based on in situ vadose zone data using mass balance, Darcy flow equation, and HYDRUS modeling.

In both growing seasons, no correlation was observed between the water flux at depth of 2.9 m and the measured mobile pore water NO_3^- concentration at that depth ($R^2 = 0.017$; $P < 0.0001$), that is, sites with high water flux did not have low pore water NO_3^- concentration or vice versa.

Discussion

Water flux

Water content measurements along the soil profile provided a key role in all the flux calculation methods applied in this study. Yet, the water-content measurement methods showed significant differences in their readings (i.e., neutron thermalization using a NP sensor and bulk soil permittivity using the 5TE capacitance and frequency domain sensor; Table 2). We hypothesize that the differences between the readings of the two methods results from two major factors: (i) soil volume measured by the sensor and (ii) installation procedure. The soil volume measured by the 5TE sensor (0.0007 m^3; Decagon Devices, 2016) is 20 to 700 times smaller than the volume measured by the NP (0.014 to 0.5 m^3; Robinson et al., 2008). In addition to the much smaller volume measured by the 5TE sensor, it is difficult and sometimes impossible to properly install it at depth of 2.9 m, which requires pushing the entire length of its semiflexible, brittle prongs into undisturbed sediment at the side wall of a borehole. It is therefore more reasonable to assume that NP readings, which sample a much larger volume of undisturbed soil profile, are more representative of the true water distribution in the subsurface, especially in the deep vadose zone, as suggested by Yao et al. (2004). However, at an orchard

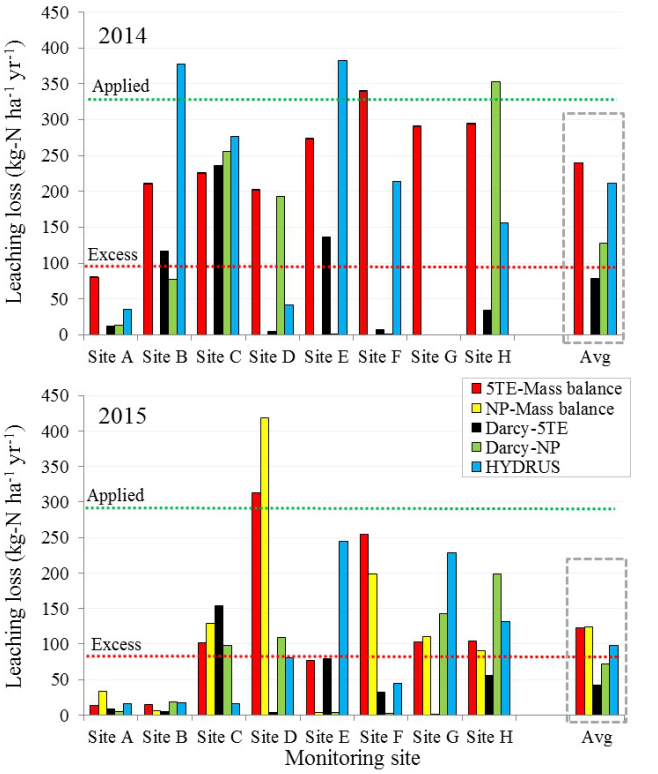

Fig. 5. Annual NO_3^-–N leaching losses below soil depth of 3 m under the monitored sites and the orchard average for the three different methods (mass balance, Darcy flow, and HYDRUS inverse modeling). Upper and lower dotted lines in each panel represent the N load applied and the annual N excess, respectively.

scale, the need for an operator and relatively slow data acquisition process makes it very hard to use NP as a tool to study the temporal dynamics (minutes to hours) of water along the vadose zone, especially over long periods. This limitation can be overcome by correlating disperse in situ NP readings with continuous in situ readings by digital sensors, such as the 5TE, installed in close proximity to the NP access tube.

Water Mass Balance

Although the annual average fluxes calculated based on the water mass balance approach (Eq. [2]) using NP and 5TE data were comparable, this method indicated substantial upward flow during the summer (5–19 cm, May–September) especially when NP data was used (Fig. 4b). We believe that these large upward water fluxes are inaccurate because of the dry conditions that prevailed in the subsurface throughout that time period (ψ less than −150 cm) and the corresponding calculated low hydraulic conductivities [$K(\psi)$ < 0.001 cm d^{-1}]. Nonuniformity in the wetting patterns of the microsprinklers in the field (most of the water falls 1.8–2.4 m away from the sprinkler, unpublished field observations) generates conditions in which only part of the infiltrating irrigation water is captured by water-content sensors. Hence, as the soil profile dries (May–October) the difference between the applied water and the observed change in storage (ΔS) increases. To sustain the mass balance, water needs to enter the upper soil profile (<3 m) from its bottom boundary (>3 m) as upward water flux (Eq. [2]). At the orchard scale, current crop coefficients (K_c) (Goldhamer, 2012) do not account for the orchard drying prior to harvest (August–September) and may lead to overestimated ET_c values, as shown in comparison with real-time measurements by an eddy covariance system (Nicolas Bambach, Department of Land, Air and Water Resources, University of California at Davis, personal communication, 2016). At the tree scale, differences exist between the orchard average ET_c values ($ET_0 \times K_c$) and the actual ET value of an individual tree, as shown by the work of Couvreur et al. (2016), who showed 5 to 8% spatial variations in root water uptake rates within and between trees in an almond orchard. Additional indication for significant within-orchard ET_c variability are the highly variable midday stem-water potentials (SWPs) across the orchard (up to 180% maximum difference, unpublished field observations). Based on the work of Johnson et al. (2005), which showed direct relations between SWP and ET_c and the observed variation in midday SWPs, it appears that individual tree ET values are needed to accurately use the mass balance approach. Further research is needed to demonstrate that field-observed, tree-to-tree variation in SWP lead to comparative tree-to-tree variation in ET_c. Another factor that may increase the uncertainty in the mass balance leaching estimates is the fact that most of the change in storage is concentrated in the top of the soil column, which is most effected by irrigation, whereas, at the bottom of the soil profile (>3 m), a small flux downward may still exist. Despite the discussed limitation of the mass balance approach methods, Min et al. (2015) have showed that this approach (Eq. [2]) can be used to estimate deep drainage under a double-cropping agrosystem [winter wheat (*Triticum aestivum* L.) and summer maize (*Zea mays* L.)] and that the estimated drainage is in good agreement with drainage obtained from numerical simulation (HYDRUS). Accordingly, one alternative approach to using the water mass balance method under orchards is to constrain upward fluxes by the unsaturated hydraulic conductivity; if we apply the constraint, $0 \leq L \leq -0.1$ cm mo^{-1}, the cumulative flux for the two growing seasons is ~42 cm yr^{-1} for both NP and 5TE data, which is in good agreement with the other methods.

Darcy Flux Estimates

Variations in the total soil water potential and gradient at the depth of 2.8 to 3 m across the orchard imply that an unsteady downward soil water flux existed to well below the effective root zone. Similar observations were reported by Min et al. (2015) down to depth of 5 m under wheat and maize fields. Both this study and the study of Min et al. (2015) suggest that to determine leaching by solving the Darcy flux at soil depth, at which gravity alone (unit gradient) drives flow, using methods such as steady-state unsaturated flow in a centrifuge (Nimmo et al., 1994), there is a need to get detailed field measurements of the matric potential at depths that go well below the effective root zone, probably deeper than 5 m.

Orchard average of cumulative leaching flux calculated based on the NP in situ retention curves were higher than those calculated based on the 5TE in situ relative saturation curves (Fig. 4b). The differences in the water-content readings of the two instruments generated less steep retention curves for the NP-based data in the loamy soils and for the 5TE-based data in the sandy soils (Supplemental Fig. S1). These differences stem from the installation procedure and the soil volume measured by the instruments as discussed above. The 5TE-based data led to steeper retention curves in the loamy soils mainly as a result of lower water content at saturation (θ_s) (Table 3), which, for a given water potential and hydraulic gradient, indicated lower unsaturated hydraulic conductivity (Eq. [4]) and decreased leaching flux (Supplemental Fig. S2).

The main limitation to the Darcy flux estimates came from its independence from daily mass balance conservation constraints. At three of the eight monitoring sites, the field-measured, saturated hydraulic conductivities (K_s) had to be lowered by up to two orders of magnitude to limit drainage flux to not exceed the applied water (especially following flood irrigation events). In all cases, the adjusted K_s values were within the range expected for the specific soil type (Clapp and Hornberger, 1978). One exception to that trend was observed in the K_s value for the 5TE measurements at Site E, where the K_s value was lower than expected by more than one order of magnitude. This deviation may be a result of the installation procedure of the 5TE sensor at that site, where fine sediment fell into the borehole during the installation and may have increased the water-content values compared with undisturbed sediment (Table 3; Site E NP vs. 5TE).

Overall, the generation of in situ retention curve, and its applicability in calculating the leaching flux based on monitoring of the hydraulic conditions in the vadose zone (matric potential and/or water content), is relatively accurate and is not biased by the uncertainty associated with tree-scale ET assessments. However, care must be taken to make sure that the leaching values are constrained by water mass balance conservation. Additional uncertainty in using field ψ measurement and a $K(\psi)$ curve to estimate the Darcy flux recharge rate derives from $\theta(\psi)$ hysteresis. Nimmo et al. (1994), using the submersible pressure outflow cell, suggested that this uncertainty would be approximately ±50%.

Inverse Modeling

Unlike the two aforementioned methods, the HYDRUS modeling approach was constrained daily by both water mass balance and hydraulic properties of the soil profile. In contrast to the Darcy method, where only the hydraulic properties of the soil layer at depths of 2.8 to 3.0 m were characterized, the inverse modeling approach used soil water status observations throughout the soil profile when optimizing the hydraulic properties for two effective types of soil layers: a higher permeable soil type for most sediments identified in the profile and a layer with lower permeability for the finest grained sediments identified (see fitted soil water content and pressure head dynamics within and below the root zone in Supplemental Fig. S3 and S4, respectively). For the deep soil layer at 2.8 to 3 m depth, the fitted parameters in the calibrated HYDRUS model were different from the RETC-predicted parameters (Table 3). In most cases, the hydraulic conductivity curves from the calibrated HYDRUS were higher than values obtained by RETC given the range of matric potentials observed in the orchard (0–700 cm). The calibrated HYDRUS model therefore generates higher leaching fluxes than the Darcy method at the same matric potentials and gradients (Supplemental Fig. S2). Accordingly, the correlation between the monthly NO_3^- fluxes calculated by the Darcy and HYDRUS methods was weak ($R^2 = 0.13$). When the NO_3^- flux was aggregated over 4 mo or more (up to a year), the correlation improved, yet it did not reach a sufficient degree of correlation ($R^2 \leq 0.48$) to allow estimate of the transient deep NO_3^- flux without any data from land surface above.

At most sites, the low permeability layers are rather thin (Fig. 2); hence, their water storage has little effect on the overall soil storage. But their hydraulic conductivity controls the leaching potential of the entire soil profile during wet soil conditions (winter through early spring). Under the dry soil conditions (summer), the coarsest

Table 3. Parameters of van Genuchten (1980) equation† used to calculate Darcy water flux at soil depth of 3 m.

	Model					Darcy 5TE				Darcy NP			
Site	α	*n*	K_s	θ_s	BF	α	*n*	K_s	θ_s	α	*n*	K_s	θ_s
A	0.0016	1.2020	31.1	0.20	89.2	0.0095	6.2847	2.4	0.19	0.3521	1.0691	71	0.41
B	0.0011	1.1505	210	0.20	78.8	0.0037	1.7034	4.8	0.27	0.0010	2.2447	3.8	0.34
C	0.0010	1.2135	198	0.20	75.5	0.0074	2.9078	4.2	0.27	0.0072	1.7820	7.0	0.34
D	0.0841	1.5893	0.71	0.32	70.0	0.1450	1.3713	21	0.32	0.0104	2.2379	21	0.08
E	0.0232	2.8485	310	0.11	76.5	0.0707	3.0150	0.63	0.13	3.8147	1.1600	500	0.13
F	0.0036	1.1678	0.22	0.21	75.1	0.0085	1.5068	14.12	0.20	0.0022	1.6270	0.07	0.35
G	0.0297	1.1803	30.0	0.34	55.3	0.2770	1.5100	30.7	0.48	0.0056	1.1760	15.4	0.32
H	0.0123	1.1590	2.74	0.18	78.1	0.2660	1.1580	8.4	0.22	0.0176	1.7264	0.56	0.08

† α, empirical parameter related to the inverse of the air entry pressure (cm^{-1}); *n*, empirical parameter represents a measure of the pore-size distribution (-); K_s, hydraulic conductivity at saturation (cm d^{-1}); θ_s, volumetric water content at saturation (-); BF, best fit (%).

soil layers will control effective vertical movement (Warrick, 2002). Furthermore, at several sites, the soils identified and measured at 2.8 to 3 m depth have different soil properties than the low permeability layers elsewhere in the 3-m profile.

At the larger orchard and annual spatiotemporal scale, the good agreement between the average annual water loss estimates by all three methods, especially after correcting the mass balance for upward flow overestimates, suggests that the use of a simple root water uptake model (Feddes et al., 1978) and one-dimensional root distribution model (Vrugt et al., 2001) in addition to the Richards flow equation was sufficient to capture the water flow dynamics at the different sites with HYDRUS. Although the same ET_c values were used for both the water mass balance and the inverse modeling approaches, the HYDRUS model did not indicate unrealistic upward flow fluxes during the summer as a result of the low hydraulic conductivity of the soil at that time. Another advantage of the HYDRUS model over the other methods is that it takes into account soil physical processes and observations across the full 3-m soil column, which therefore allows for predictive analyses that could be used to minimize leaching via optimizing the irrigation and fertigation management and to evaluate impacts of winter precipitation and nutrient management options in the early season.

Orchard Scale Nitrate Loss Estimates

Comparison between the measured orchard-scale annual N excess (applied N minus harvested N) and the annual N losses below the root zone computed by the three aforementioned methods indicates up to threefold difference in the N losses (Fig. 5). Based on the work of Baram et al. (2016), which showed that the N load in the soil at that research site did not change significantly between the two growing seasons, the orchard average annual N excess served as good and inexpensive approximation of the maximal N load available annually for leaching. However, the differences in N removal observed at the tree or tree-row scale suggest high spatial variability in N excess within the orchard. The work of Silva et al. (2013), which studied multiple almond orchards for 4 yr, shows similar variability in yield and N contents. Tree- and tree-row-scale spatial variability in N excess may explain the high spatial variability in pore water NO_3^- concentration at depth of 2.9 m (Fig. 3) and the differences between the annual N losses at the different monitoring sites (Fig. 5).

When totaled over the year and averaged across the orchard (upscaling), good agreement is achieved for orchard-annual-scale N losses to below the root zone between the vadose-zone-based estimates and the orchard annual N excess (orchard N mass balance). This indicates that at this research site, eight vadose zone monitoring sites, with different soil layering, were sufficient to capture the spatial variability in N losses at the orchard scale and that upscaling by averaging across space and time provides adequate results.

Orchard management at our research site included a prebloom refill of the soil water storage, which, mainly in the early growing season, lead to N leaching losses from the root zone while the soil profile was wet (February through early May). This management practice prevents long-term N buildup in the upper 3 m of the soil profile by increasing N losses during early season fertilizer applications (Baram et al., 2016). Alternatively, under orchard irrigation management that minimizes water-leaching losses, N would accumulate in the upper 3 m of the soil profile, similar to the natural buildup of N in arid and semiarid regions (Stone and Edmunds, 2014). Under those conditions, pore water sampling at 3 m depth or immediately below the effective root zone may not be representative of the annual soil N buildup, as observed by Baram et al. (2016) under a pistachio orchard in the same region.

In either case, it is difficult to determine a priori the number of monitoring sites needed for appropriate upscaling to the orchard scale as a function of spatial variability in soil properties. Indication to the limitation of predetermined number of soil sampling sites to represent mean field NO_3^- content was presented by Ilsemann et al. (2001). The use of 3-D heterogeneous modeling that accounts for the 3-D distribution of the root system, the variability in microsprinkler wetting, and the heterogeneity of the porous medium (Russo et al., 2013) or the use of remote sensing to characterize spatial heterogeneity in water uptake within an orchard (Bellvert et al., 2016) may assist in identifying areas with high and low leaching potentials (i.e., low and high water uptake, respectively), which, in turn may improve the selection of monitoring sites within an orchard, increase the accuracy of leaching estimates from an orchard, and drive precision irrigation applications.

While it appears feasible to estimate annual N and water losses from mass balance or vadose zone monitoring and modeling data, our results also indicate that it is much harder to estimate the orchard average NO_3^- concentration in the pore water leaching below the effective root zone. Using simple mass balance of N and water [(N applied − N removed)/(rain + irrigation − ET_c)] indicates that the average NO_3^-–N concentrations in the leaching water should have been 38 and 143 mg L^{-1} for the 2014 and 2015 growing seasons, respectively (Table 1). When the same annual N excess for 2014 and 2015 is divided instead by the corresponding annual water leaching amount estimated by the aforementioned methods, NO_3^-–N concentrations are estimated as follows: for water mass balance (Eq. [2]), 59 and 45 to 39 mg L^{-1}, respectively; for Darcy method (Eq. [4]), 71 to 55 and 82 to 51 mg L^{-1}, respectively; and for HYDRUS modeling, 31.6 and 45.3 mg L^{-1}, respectively. These NO_3^-–N concentrations are lower than the average measured concentrations in the pore water samples (109 and 75 mg L^{-1} in 2014 and 2015, respectively). Differences likely are due to assuming uniform boundary conditions across the orchard. In reality, spatial variability in N uptake under uniform N applications along with the dominance of preferential flow and N transport at the orchard scale causes highly variable NO_3^-–N concentrations (Baram et al., 2016; Onsoy et al., 2005;

Russo et al., 2013). Identification and quantification of high and low productivity zones within an orchard may be used to improve N losses estimates as previously suggested by Delgado et al. (2005) for irrigated cornfields.

Capturing flood flows for groundwater recharge by flooding private farmlands in the San Joaquin Valley has been suggested as a means to improve and replenish aquifers over the long term (Bachand et al., 2014). Based on the data presented in this manuscript, and the working assumption of 70% N use efficiency in almond orchards using best management practices (Silva et al., 2013), N excess of 60 to 100 kg N ha^{-1} annually accumulates in the soil profile below the root zone of almond orchards. To comply with drinking standards (10 mg NO_3^-–N L^{-1}) 0.68 to 1.0 m of clean flood water recharge would be needed to dilute the NO_3^- concentrations to drinking water standards. Lower recharge, such as 2.5 to 10 cm (1 to 4 inch), would lead to NO_3^-–N concentrations in the propagating pore water to be an order of magnitude higher than the groundwater drinking standards. With more precise management practices, N use efficiencies in excess of 90% are conceivable (as shown for other perennial tree crops (Neilsen and Neilsen, 2002), in which case, N loading would be reduced to <30 kg N ha^{-1}. Matching this with winter flood recharge of 30 cm would be sufficient to reduce recharge NO_3^- concentrations to levels below the drinking water limit.

Conclusions

This study used eight sites of intensive vadose zone monitoring. Averaging and totalizing across the eight sites as a means to upscale the local data was appropriate for estimating the annual orchard average N loss through deep (>3 m) leaching. Neutron probe readings were found to be more representative of the soil water content profile than 5TE sensors because of larger measuring volume and ease of installation. Nonetheless, 5TE data provide valuable continuous data on the water dynamics in the soil profile. Despite the huge spatial variability in the NO_3^- concentration, the orchard average annual N losses obtained from four methods—the orchard N mass balance, the orchard water mass balance, flow calculations, and HYDRUS modeling—were all of similar high magnitude (80–240 kg N ha^{-1} y^{-1}). Better knowledge of tree-based ET data is needed to prevent overestimated upward flow in the water mass balance approach. Extreme wetting events can be used in Darcy flux estimates to validate field measured saturated hydraulic conductivities (K_s). The study indicated that simple N excess obtained from mass balance (i.e., N load applied minus N load removed) provides a good proxy of the annual N accumulation in the soil profile. Under typical current best management practices, the N load to groundwater is likely in the range of 60 to 100 kg N ha^{-1}.

Acknowledgments

We acknowledge funding from the California Department of Food and Agriculture's Fertilizer Research and Education Program (CDFA-FREP) through project 12-0454-SA, by the Almond Board of California through project number 13PREC6SMART, and by the California Pistachio Research Board through project number 2013-02890. During the preparation of this manuscript, V.C. was supported by the Belgian American Educational Foundation (BAEF) as UC-Louvain Fellow, by Wallonie-Bruxelles International (WBI) with a WBI.WORLD excellence grant, and by the *Fonds Spéciaux de Recherche* (FSR) of the *Université Catholique de Louvain*.

References

Almasri, M.N., and J.J. Kaluarachchi. 2004. Assessment and management of long-term nitrate pollution of ground water in agriculture-dominated watersheds. J. Hydrol. 295:225–245. doi:10.1016/j.jhydrol.2004.03.013

California Almond Sustainability Program. 2016. Online nitrogen calculator. https://www.sustainablealmondgrowing.org/Home/tabid/71/ctl/Edit/mid/628/Default. (accessed 29 Sept. 2016).

American Public Health Association. 1998. Standard methods for the examination of water and wastewater. 20th ed. United Book Press, Baltimore, MD.

Ashworth, J., D. Keyes, R. Kirk, and R. Lessard. 2001. Standard procedure in the hydrometer method for particle size analysis. Commun. Soil Sci. Plant Anal. 32:633–642. doi:10.1081/CSS-100103897

Bachand, P.A.M., S.B. Roy, J. Choperena, D. Cameron, and W.R. Horwath. 2014. Implications of using on-farm flood flow capture to recharge groundwater and mitigate flood risks along the Kings River, CA. Environ. Sci. Technol. 48:13601–13609. doi:10.1021/es501115c

Baram, S., V. Couvreur, T. Harter, M. Read, P.H. Brown, J.W. Hopmans, and D.R. Smart. 2016. Assessment of orchard N losses to groundwater with a vadose zone monitoring network. Agric. Water Manage. 172:83–95. doi:10.1016/j.agwat.2016.04.012

Bellvert, J., J. Marsal, J. Girona, V. Gonzalez-Dugo, E. Fereres, S. Ustin, and P. Zarco-Tejada. 2016. Airborne thermal imagery to detect the seasonal evolution of crop water status in peach, nectarine and Saturn peach orchards. Remote Sens. 8:39. doi:10.3390/rs8010039

Botros, F.E., Y.S. Onsoy, T.R. Ginn, and T. Harter. 2012. Richards equation–based modeling to estimate flow and nitrate transport in a deep alluvial vadose zone. Vadose Zone J. 11. doi:10.2136/vzj2011.0145

California Environmental Protection Agency. 2000. Hydrogeologically vulnerable areas map. CalEPA, State Water Resources Control Board, Sacramento, CA. http://www.waterboards.ca.gov/gama/docs/hva_map_table.pdf (accessed 20 Aug. 2015).

California Irrigation Management and Information System. 2014. CIMIS overview. California Dep. of Water Resources, CIMIS, Fresno, CA. http://www.cimis.water.ca.gov/Default.aspx (accessed 29 Sept. 2016).

California Soil Resource Lab. 2015. SoilWeb: Interactive map of USDA–NCSS soil survey data for locations throughout most of the US. Calif. Soil Resour. Lab., Univ. of California–Davis, and Univ. of California Div. Agric. Natural Resour. in collaboration with USDA–NRCS. http://casoilresource.lawr.ucdavis.edu/gmap/ (accessed 20 Aug. 2015).

Clapp, R.B., and G.M. Hornberger. 1978. Empirical equations for some soil hydraulic properties. Water Resour. Res. 14:601–604. doi:10.1029/WR014i004p00601

Coleman, T.F., and Y. Li, 1996. An interior trust region approach for nonlinear minimization subject to bounds. SIAM J. Optim. 6:418–445. doi:10.1137/0806023

Couvreur, V., M.M. Kandelous, B.L. Sanden, B.D. Lampinen, and J.W. Hopmans. 2016. Downscaling transpiration rate from field to tree scale. Agric. For. Meteorol. 221:71–77. doi:10.1016/j.agrformet.2016.02.008

Decagon Devices. 2016. 5TE Soil moisture, temperature, and electrical conductivity sensor. Decagon Devices, Inc., Pullman, WA. https://www.decagon.com/en/soils/volumetric-water-content-sensors/5te-vwc-temp-ec/ (accessed 13 May 2016).

Delgado, J.A., R. Khosla, W.C. Bausch, D.G. Westfall, and D.J. Inman. 2005. Nitrogen fertilizer management based on site-specific management zones reduces potential for nitrate leaching. J. Soil Water Conserv. 60:402–410.

Doane, T.A., and W.R. Horwáth. 2003. Spectrophotometric determination of nitrate with a single reagent. Anal. Lett. 36:2713–2722. doi:10.1081/AL-120024647

Dowd, B.M., D. Press, and M.L. Huertos. 2008. Agricultural nonpoint source water pollution policy: The case of California's Central Coast. Agric. Ecosyst. Environ. 128:151–161. doi:10.1016/j.agee.2008.05.014

Drevno, A., 2016. Policy tools for agricultural nonpoint source water pollution control in the U.S. and E.U. Manage. Environ. Quality 27:106–123. doi:10.1108/MEQ-12-2014-0177.

Feddes, R.A., P.J. Kowalik, and H. Zaradny. 1978. Simulation of field water use and crop yield. Wiley, New York.

Fraters, D., A.W.F. Veldstra, F.M.L. Vaessen, J.W.A.M. Crijns, L.J.M. Boumans, and P.J.J.M. Kusters. 2016. Use of early warning monitoring systems for groundwater protection in a policy decision context. In: Abstracts, To-

ward Sustainable Groundwater in Agriculture: 2nd International Conference Linking Science and Policy, Burlingame, CA. 28–30 June 2016. Water Educ. Foundation, Sacramento, CA, and Univ. California–Davis.

Gärdenäs, A.I., J.W. Hopmans, B.R. Hanson, and J. Šimůnek. 2005. Two-dimensional modeling of nitrate leaching for various fertigation scenarios under micro-irrigation. Agric. Water Manage. 74:219–242. doi:10.1016/j.agwat.2004.11.011

Giebel, A., O. Wendroth, H. Isaak Reuter, K.C. Kersebaum, and J. Schwarz. 2006. How representatively can we sample soil mineral nitrogen? J. Plant Nutr. Soil Sci. 169:52–59. doi:10.1002/jpln.200521755

Goldhamer, D. 2012. Yield response to water in fruit trees and vines: Guidelines. In: P. Steduto, T.C. Hsiao, E. Fereres, and D. Raes, editors, FAO Irrigation and Drainage Paper No. 66. Food and Agriculture Organization of the United Nations, Rome, Italy. p. 358–375.

Green, C.T., L.H. Fisher, and B.A. Bekins. 2008. Nitrogen fluxes through unsaturated zones in five agricultural settings across the United States. J. Environ. Qual. 37:1073–1085. doi:10.2134/jeq2007.0010

Hallberg, G. 1987. The impacts of agricultural chemicals on ground water quality. GeoJournal 15:283–295. doi:10.1007/BF00213456

Harter, T., Y. Onsoy, K. Heeren, M. Denton, G. Weissmann, J. Hopmans, and W. Horwath. 2005. Deep vadose zone hydrology demonstrates fate of nitrate in eastern San Joaquin Valley. Calif. Agric. 59:124–132. doi:10.3733/ca.v059n02p124

Healy, R.W., and B.R. Scanlon. 2010. Estimating groundwater recharge. Cambridge Univ. Press, Cambridge. doi:10.1017/CBO9780511780745

Huang, J., J. Xu, X. Liu, J. Liu, and L. Wang. 2011. Spatial distribution pattern analysis of groundwater nitrate nitrogen pollution in Shandong intensive farming regions of China using neural network method. Math. Comput. Model. 54:995–1004. doi:10.1016/j.mcm.2010.11.027

Ilsemann, J., Goeb, S., Bachmann, J., 2001. How many soil samples are necessary to obtain a reliable estimate of mean nitrate concentrations in an agricultural field? J. Plant Nutr. Soil Sci. 164:585–590. doi:10.1002/1522-2624(200110)164:5<585::AID-JPLN585>3.0.CO;2-M

Johnson, R., L. Williams, J. Ayars, and T. Trout. 2005. Weighing lysimeters aid study of water relations in tree and vine crops. Calif. Agric. 59:133–136. doi:10.3733/ca.v059n02p133

Kempers, A.J., and C.J. Kok. 1989. Re-examination of the determination of ammonium as the indophenol blue complex using salicylate. Anal. Chim. Acta 221:147–155. doi:10.1016/S0003-2670(00)81948-0

Kendrick, K.J., and R.C. Graham. 2004. Pedogenic silica accumulation in chronosequence soils, southern California. Soil Sci. Soc. Am. J. 68:1295–1303. doi:10.2136/sssaj2004.1295

Kurtzman, D., R.H. Shapira, A. Bar-Tal, P. Fine, and D. Russo. 2013. Nitrate fluxes to groundwater under citrus orchards in a Mediterranean climate: Observations, calibrated models, simulations and agro-hydrological conclusions. J. Contam. Hydrol. 151:93–104. doi:10.1016/j.jconhyd.2013.05.004

Lagarias, J.C., J.A. Reeds, M.H. Wright, P.E. Wright. 1998. Convergence properties of the Nelder–Mead simplex method in low dimensions. SIAM J. Optim. 9, 112–147. doi:10.1137/S1052623496303470

Li, X., C. Hu, J.A. Delgado, Y. Zhang, and Z. Ouyang. 2007. Increased nitrogen use efficiencies as a key mitigation alternative to reduce nitrate leaching in north china plain. Agric. Water Manage. 89:137–147. doi:10.1016/j.agwat.2006.12.012

MathWorks. 2012. MATLAB 8.0 and statistics toolbox 8.1, The MathWorks, Inc., Natick, Massachusetts, United States.

Min, L., Y. Shen, and H. Pei. 2015. Estimating groundwater recharge using deep vadose zone data under typical irrigated cropland in the piedmont region of the North China Plain. J. Hydrol. 527:305–315. doi:10.1016/j.jhydrol.2015.04.064

Mohanty, B., and R. Kanwar. 1994. Spatial variability of residual nitrate-nitrogen under two tillage systems in central Iowa: A composite three-dimensional resistant and exploratory approach. Water Resour. Res. 30:237–251. doi:10.1029/93WR02922

Mualem, Y. 1976. A new model for predicting the hydraulic conductivity of unsaturated porous media. Water Resour. Res. 12:513–522. doi:10.1029/WR012i003p00513

Neilsen, D., and G.H. Neilsen. 2002. Efficient use of nitrogen and water in high-density apple orchards. Horttechnology 12:19–25.

Nimmo, J.R., D.A. Stonestrom, and K.C. Akstin. 1994. The feasibility of recharge rate determinations using the steady-state centrifuge method. Soil Sci. Soc. Am. J. 58:49–56. doi:10.2136/sssaj1994.03615995005800010007x

Onsoy, Y.S., T. Harter, T.R. Ginn, and W.R. Horwath. 2005. Spatial variability and transport of nitrate in a deep alluvial vadose zone. Vadose Zone J. 4:41–54. doi:10.2113/4.1.41

Page, R.W., 1986. Geology of the fresh ground-water basin of the Central Valley, California, with texture maps and sections. Professional Paper USGS 1401-C. Plate 4. USGS, Reston, VA.

Richards, L.A. 1931. Capillary conduction of liquids through porous mediums. J. Appl. Phys. 1:318–333. doi:10.1063/1.1745010

Robinson, D.A., C.S. Campbell, J.W. Hopmans, B.K. Hornbuckle, S.B. Jones, R. Knight, F. Ogden, J. Selker, and O. Wendroth. 2008. Soil moisture measurement for ecological and hydrological watershed-scale observatories: A Review. Vadose Zone J. 7:358–389. doi:10.2136/vzj2007.0143

Russo, D., A. Laufer, R.H. Shapira, and D. Kurtzman. 2013. Assessment of solute fluxes beneath an orchard irrigated with treated sewage water: A numerical study. Water Resour. Res. 49:657–674. doi:10.1002/wrcr.20085

Silva, S.S., M. Saiful, B. Sanden, E. Laca, and P. Brown. 2013. Almond early-season sampling and in-season nitrogen application maximizes productivity, minimizes loss: Protocol for early-season sampling and in-season nitrogen budgeting. Almond Board, Modesto, CA. http://ucanr.edu/sites/scri/files/189631.pdf (accessed 29 Sept. 2016).

Šimůnek, J., M. Šejna, and M.Th. van Genuchten. 1998. The Hydrus-1D software package for simulating the one-dimensional movement of water, heat, and multiple solutes in variably-saturated media. Version 2.0, IGWMC-TPS-70. International Ground Water Modeling Center, Colorado School of Mines, Golden, CO.

Spalding, R.F., and M.E. Exner. 1993. Occurrence of nitrate in groundwater: A review. J. Environ. Qual. 22:392–402. doi:10.2134/jeq1993.00472425002200030002x

Stenger, R., E. Priesack, and F. Beese. 2002. Spatial variation of nitrate-N and related soil properties at the plot-scale. Geoderma 105:259–275. doi:10.1016/S0016-7061(01)00107-0

Stone, A.E.C., and W.M. Edmunds. 2014. Naturally-high nitrate in unsaturated zone sand dunes above the Stampriet Basin, Namibia. J. Arid Environ. 105:41–51. doi:10.1016/j.jaridenv.2014.02.015

Tsakiris, G. 2015. The status of the European waters in 2015: A Review. Environ. Processes 2:543–557. doi:10.1007/s40710-015-0079-1

Turkeltaub, T., D. Kurtzman, and O. Dahan. 2016. Real-time monitoring of nitrate transport in deep vadose zone under a crop field– implications for groundwater protection. Hydrol. Earth Syst. Sci. Discuss. 20:3099–3108. doi:10.5194/hess-2016-63

Turkeltaub, T., D. Kurtzman, E.E. Russak, and O. Dahan. 2015. Impact of switching crop type on water and solute fluxes in deep vadose zone. Water Resour. Res. 51:9828–9842. doi:10.1002/2015WR017612

US Bureau of Reclamation–Denver. 1990. Earth manual part 2, 3rd ed. USBR, Materials Engineering Branch. US Gov. Print. Office, Denver, CO.

van Genuchten, M.Th. 1980. A closed-form equation for predicting the hydraulic conductivity of unsaturated soils, A- vg.pdf. Soil Sci. Soc. Am. J. 44:892–898. doi:10.2136/sssaj1980.03615995004400050002x

van Genuchten, M.Th., F. Leij, and S. Yates. 1991. The RETC code for quantifying the hydraulic functions of unsaturated soils. EPA/600/2-91/065. Robert S. Kerr Environ. Research Lab., Office of Research and Development, USEPA, Ada, OK

Viers, J.H., D. Liptzin, T.S. Rosenstock, V.B. Jensen, A.D. Hollander, A. McNally, A.M. King, G. Kourakos, E.M. Lopez, N. De La Mora, A. Fryjoff-Hung, K.N. Dzurella, H. Canada, S. Laybourne, C. McKenney, J. Darby, J.F. Quinn, and T. Harter. 2012. Addressing nitrate in California's drinking water: Technical Report 2: Nitrogen sources and loading to groundwater. Center for Watershed Sciences, University of California, Davis.

Vrba, J., and B. Adams, editors. 2008. Groundwater early warning monitoring strategy: A methodological guide. UNESCO, Paris.

Vrugt, J.A., M.T. van Wijk, J.W. Hopmans, and J. Šimunek. 2001. One-, two-, and three-dimensional root water uptake functions for transient modeling. Water Resour. Res. 37:2457–2470. doi:10.1029/2000WR000027

Warrick, A.W. 2002. Soil physics companion. CRC Press, Boca Raton, FL.

Weissmann, G.S., Y. Zhang, G.E. Fogg, and J.F. Mount. 2004. Influence of incised-valley-fill deposits on hydrogeology of a stream-dominated alluvial fan. In: J.S. Bridge and D. Hyndman, editors, Aquifer characterization. Special Publications of SEPM. Vol. 80. Society for Sedimentary Geology, Tulsa, OK. p. 15–28. doi:10.2110/pec.04.80.0015

Whitley, D., 1994. A genetic algorithm tutorial. Stat. Comput. 4:65–85. doi:10.1007/BF00175354

Yao, T., P.J. Wierenga, A.R. Graham, and S.P. Neuman. 2004. Neutron probe calibration in a vertically stratified vadose zone. Vadose Zone J. 3:1400–1406.